JNTM JOURNAL of NEW TECHNOLOGY and MATERIALS

Journal of New Technology and Materials

Vol. 13, No. 2 (2023), 27–38

RESEARCH ARTICLE

Load-Adaptive Energy–Transport Normalization of Printed Glucose-Oxidase Biofuel Cells for Flexible Self-Powered Sweat Biosensing

Vincent Marks[1,*]

[1]University of Surrey, Guildford GU2 7XH, Surrey, UK

*Correspondence: vincentmarks@btinternet.com

Received date: March 28, 2023; Accepted date: October 20, 2023

Abstract

Wearable enzymatic biofuel cells are often described by isolated quantities such as open-circuit voltage, maximum power density, or analyte sensitivity, although their practical performance is governed by the simultaneous coupling of load selection, enzyme affinity, transport state, sweat composition, and mechanical deformation. This paper develops a load-adaptive energy–transport normalization of a flexible printed glucose-oxidase biofuel cell in which naphthoquinone/multiwalled-carbon-nanotube and Prussian-blue/multiwalled-carbon-nanotube nanocomposites form the bioanode and biocathode, respectively. The analysis treats maximum-power operation, resistance-area matching, apparent Michaelis compatibility, scan-rate-derived transport behavior, artificial-sweat voltage calibration, interferent tolerance, and bending endurance as mutually dependent descriptors of one self-powered sensing material. At 20 mM glucose, the cell produces 266 $\mu W\,cm^{-2}$ at 0.20 V, giving a maximum-power current density of 1.33 $mA\,cm^{-2}$, an area-normalized external-load requirement of 150 $\Omega\,cm^2$, and an internal-loss term of 188 $\Omega\,cm^2$. Apparent Michaelis constants of 2.47 mM for the bioanode and 2.99 mM for the biocathode yield a kinetic-balance factor of 0.995, showing that the single-enzyme electrode pair remains closely matched over the same low-millimolar glucose window. The artificial-sweat voltage response follows a saturating calibration with $R^2 = 0.9737$, while the printed film retains more than 83% of electrochemical response after 100 repeated 180° bending cycles. These results answer the central question by showing that the device is not merely a high-power flexible biofuel cell; it is a load-sensitive, transport-limited, mechanically recoverable nanocomposite transducer whose reliable biosensing operation requires calibration under the same load and deformation conditions intended for use.

Keywords: Flexible materials, glucose oxidase, enzymatic biofuel cell, self-powered biosensor, Prussian blue, carbon nanotube electrode, wearable electrochemistry

1 Introduction

Flexible electrochemical bioelectronics are moving from rigid benchtop sensors toward thin, deformable systems that can operate on skin, in textiles, and in other soft interfaces where the sample volume is limited and the mechanical environment changes continuously. In such settings, the energy budget of the sensor is not a secondary matter. The device must often detect a metabolite, condition the signal, and communicate or store the result while remaining conformable, lightweight, and safe for direct contact with biological fluids. Enzymatic biofuel cells are therefore attractive for wearable biosensing because the target or coexisting metabolite can function as both biochemical fuel and analytical input, allowing signal generation without an externally imposed sensing bias [1, 2]. Recent work on wearable enzyme-based devices has emphasized that electrode materials, enzyme immobilization, and system integration must be considered together, rather than as separate optimization problems [3].

Glucose remains one of the most important fuels for self-powered biosensing because glucose oxidase is chemically well established, selective, commercially accessible, and compatible with mild aqueous media. The enzymatic oxidation of glucose provides a route to autonomous current generation, while the resulting voltage or current can be correlated

with analyte concentration. For wearable operation, however, the problem is more demanding than conventional glucose sensing. Sweat glucose concentrations are lower and more variable than blood glucose concentrations, ionic composition changes with perspiration rate, and interferents such as lactate, uric acid, ascorbic acid, creatinine, chloride, and carbonate species can affect local electrochemical conditions [4, 5]. The device must therefore generate a readable glucose-dependent signal in a complex electrolyte while preserving function under bending and partial dehydration.

The literature on enzymatic biofuel cells has shown several strategies for improving output, including direct-electron-transfer designs, mediated-electron-transfer designs, porous carbon scaffolds, metal/metal-oxide nanostructures, conductive polymers, and hybrid nanocarbon networks [6]. For glucose oxidase, direct electron transfer is intrinsically challenging because the flavin adenine dinucleotide redox center is embedded within the protein structure, so mediated pathways and high-surface-area conductive supports often provide more reliable current collection [7, 8]. Naphthoquinone-modified carbon nanotube films can assist anodic glucose oxidation, whereas Prussian-blue-based films are widely used for low-potential hydrogen peroxide electrocatalysis and can support the cathodic branch of a single-enzyme architecture [9, 10]. These materials considerations are especially relevant in printed devices because the active layer must simultaneously provide redox mediation, enzyme hosting, electronic percolation, mechanical compliance, and wet-state ion transport.

Screen-printable nanocomposite inks have become a practical route for such multifunctional electrode films. They allow carbon nanotubes, graphite, mediators, electrocatalysts, polymer binders, and enzymes to be combined in a format compatible with low-cost flexible substrates and scalable patterning. The printed single-enzyme glucose biofuel-cell architecture examined here is consistent with this direction: the bioanode contains a naphthoquinone/multiwalled-carbon-nanotube network, while the biocathode contains a Prussian-blue/multiwalled-carbon-nanotube hybrid, and glucose oxidase is immobilized at both electrodes [11]. This design is attractive because it avoids the additional biochemical complexity of pairing two different enzymes, but it also creates a stringent requirement: the anodic and cathodic branches must remain kinetically compatible within the same glucose concentration interval.

Several recent reviews have identified self-powered sweat sensors and textile biofuel cells as promising platforms for non-invasive personal monitoring, but they also emphasize unresolved barriers in stability, calibration, power management, and real-sample operation [12, 13]. A central weakness in many device reports is that the biofuel cell is described using a small set of independent metrics: open-circuit voltage, maximum power density, sensor sensitivity, linear range, or bending retention. These values are useful but incomplete. Open-circuit voltage does not specify a usable load. Maximum power does not determine the most stable analytical readout. High enzyme activity at one electrode does not guarantee balanced cell operation. Bending retention does not prove that calibration remains unchanged after deformation. For a wearable self-powered biosensor, these quantities must be interpreted as a coupled materials-and-circuit system.

The research question addressed in this paper is therefore specific: can a flexible printed single-enzyme glucose biofuel cell be evaluated through a load-adaptive normalization that simultaneously explains power delivery, kinetic matching, transport behavior, artificial-sweat voltage calibration, selectivity, and mechanical endurance? The answer is sought not by introducing a new experimental architecture, but by converting the measured operating quantities of the printed nanocomposite device into interpretable resistance-area, kinetic-balance, transport-compatibility, and deformation-aware sensing descriptors. This approach gives the paper a materials-centered contribution: it relates the chemistry and morphology of the printed electrodes to the external load and to the calibration conditions under which the self-powered sweat sensor should actually be used.

2 Materials and methodology

2.1 Material platform and measured operating quantities

The device considered here is a flexible two-electrode glucose biofuel cell fabricated from printed nanocomposite films. The bioanode contains naphthoquinone, multiwalled carbon nanotubes, graphite, and polyurethane, whereas the biocathode contains a Prussian-blue/multiwalled-carbon-nanotube hybrid, graphite, and polyurethane. Glucose oxidase is immobilized at both electrodes. At the bioanode, glucose oxidation is coupled to mediated electron transfer through the naphthoquinone/carbon network. At the biocathode, glucose oxidase generates hydrogen peroxide that is reduced electrocatalytically at the Prussian-blue-containing composite. The paired mechanism allows glucose to serve as the common biochemical input for fuel conversion and autonomous sensing.

Figure 1 is important because it shows that the subsequent electrical descriptors are not abstract circuit parameters detached from the material geometry. The printed conductor traces, narrow inter-electrode spacing, and distinct anodic and cathodic film regions define the current pathway and the wet electrochemical volume. The black anodic film and blue cathodic film also mark the two different redox chemistries that must remain coordinated during glucose oxidation, peroxide formation, and cathodic reduction. Any interpretation of load, transport, or bending must therefore be tied to this physically asymmetric but functionally coupled layout.

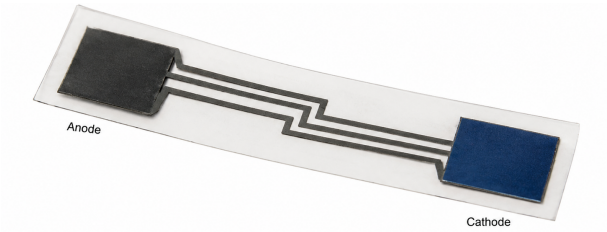

Figure 1. Printed flexible glucose biofuel-cell layout showing the dark naphthoquinone/MWCNT bioanode, the blue Prussian-blue/MWCNT biocathode, and the current-collector traces on a transparent flexible substrate. The compact geometry places the two enzyme-functionalized nanocomposites in the same glucose-containing medium so that energy conversion and voltage readout arise from one shared electrochemical environment.

The measured quantities used for normalization are summarized in Table 1. The numerical record includes maximum-power operation at 20 mM glucose, glucose-power calibration, self-powered current sensing, artificial-sweat voltage calibration, apparent Michaelis constants for both electrodes, cathodic peroxide response, and repeated bending endurance. The values are drawn together so that the flexible device can be analyzed as one integrated material system rather than as a collection of unrelated measurements.

Table 1. Measured and fitted operating quantities used for load-adaptive energy–transport normalization of the flexible glucose biofuel cell.

Category	Quantity	Value used
Cell-level energy output	Open-circuit voltage at 20 mM glucose	0.45 V
Cell-level energy output	Maximum power density	266 µW cm^{-2}
Cell-level energy output	Voltage at maximum power	0.20 V
Cell-level energy output	Approximate current density at high glucose	1.3 mA cm^{-2}
Power calibration	Glucose interval for areal-power calibration	0 mM to 20 mM
Power calibration	Power sensitivity	2.1(1) µW cm^{-2} mM^{-1}
Self-powered current sensing	Glucose interval	0 mM to 10 mM
Self-powered current sensing	Linear segment and sensitivity	up to 1.5 mM;0.026(4) µA cm^{-2} mM^{-1}
Artificial-sweat voltage sensing	Glucose interval	0 mM to 10 mM
Artificial-sweat voltage sensing	Nonlinear calibration quality	$R^2 = 0.9737$
Bioanode kinetics	Apparent Michaelis constant	2.47 mM
Biocathode kinetics	Apparent Michaelis constant	2.99 mM
Biocathode peroxide response	Linear hydrogen peroxide interval and sensitivity	0.25 mM to 10 mM; 9.76 µA mM^{-1}
Mechanical endurance	Bending at 180°	150 cycles examined; >83% retained after 100 cycles

Table 1 defines the analytical boundary of the paper. The same set of quantities spans power extraction, enzyme kinetics, voltage readout, interferent tolerance, and deformation response, so it permits a direct comparison between energy-harvesting and biosensing requirements. The table also shows why a single headline value cannot represent the device: maximum power is determined at high glucose and a specific voltage, whereas sweat sensing is evaluated over 0 mM to 10 mM glucose and is governed by a nonlinear voltage curve. This distinction motivates the normalization developed below.

2.2 Load-adaptive energy–transport normalization

The maximum-power current density was obtained from the areal power density and the cell voltage at the maximum-power point:

$$j_{\mathrm{mp}} = \frac{P_{\max}}{E_{\mathrm{mp}}}. \tag{1}$$

Eq. (1) converts a power-density result into the current density that the printed electrode pair must actually sustain under load. This step is necessary because a flexible biofuel cell may display a favorable power density while still operating at a current density that imposes substantial transport, mediator-turnover, and percolation demands on the soft electrode film. Here, the conversion identifies the current-delivery state associated with the power maximum rather than treating power density as an isolated scalar.

The external load required to operate near this point was expressed as an area-normalized load term:

$$r_{\mathrm{L,mp}} = \frac{E_{\mathrm{mp}}}{j_{\mathrm{mp}}}. \tag{2}$$

Eq. (2) translates the electrochemical operating point into a circuit-facing resistance-area quantity. This form is more useful than a bare resistance because printed electrodes may be scaled by changing active area, and the external electronics must be matched to current density rather than to total current alone. The term therefore connects materials performance to practical readout design.

The voltage loss between open circuit and the maximum-power condition was represented by an internal-loss term:

$$r_{\mathrm{int}} = \frac{E_{\mathrm{OC}} - E_{\mathrm{mp}}}{j_{\mathrm{mp}}}. \tag{3}$$

Eq. (3) should not be read as a purely ohmic resistance. In an enzymatic printed film it is a lumped descriptor of reaction polarization, substrate transport, mediator accessibility, ionic conduction, contact resistance, and cathodic peroxide conversion. Its value is therefore useful for comparing device states, but its physical meaning is broader than a metal-wire resistance.

Kinetic compatibility between the two glucose-oxidase electrodes was evaluated with a symmetric affinity-matching factor:

$$\Theta_K = \frac{2\sqrt{K_{m,a}^{\mathrm{app}} K_{m,c}^{\mathrm{app}}}}{K_{m,a}^{\mathrm{app}} + K_{m,c}^{\mathrm{app}}}, \tag{4}$$

where $K_{m,a}^{\mathrm{app}}$ and $K_{m,c}^{\mathrm{app}}$ are the apparent Michaelis constants of the bioanode and biocathode. Eq. (4) is constructed so that the value approaches unity only when the two apparent affinities are close. This is an appropriate descriptor for a single-enzyme biofuel cell because both electrodes consume or transduce the same glucose pool. If one branch saturated much earlier than the other, the cell would be limited by kinetic imbalance rather than by total enzyme loading alone.

Scan-rate behavior was expressed through a diffusion-compatibility index:

$$\Psi_q = 1 - \frac{|b_q - 0.5|}{0.5}, \qquad 0 \le \Psi_q \le 1, \tag{5}$$

where b_q is the exponent obtained from current–scan-rate scaling. Eq. (5) maps the familiar diffusion-like exponent of 0.5 to a value near one and assigns lower values as the behavior shifts toward more surface-associated or capacitive response. The index is not intended to replace full transport modelling; rather, it provides a compact way to compare the anodic and cathodic films using the same scale.

The glucose-voltage response in artificial sweat was fitted with a Michaelis-type saturation expression:

$$E(C) = E_0 + \frac{\Delta E_{\max} C}{K_E + C}, \tag{6}$$

where $E(C)$ is the self-generated voltage, C is glucose concentration, E_0 is the load-dependent offset, $\Delta E_{\max}$ is the maximum incremental voltage, and K_E is the concentration giving half of that incremental voltage. Eq. (6) is interpreted here as a device-level calibration law, not as a direct measurement of enzyme affinity. It contains contributions from enzymatic turnover, load selection, electrode polarization, cathodic peroxide consumption, and the ionic composition of artificial sweat.

3 Results and discussion

3.1 Load-matched energy conversion

Using the values in Table 1, Eq. (1) gives $j_{\mathrm{mp}} = 1.33\,\mathrm{mA\,cm^{-2}}$ from $266\,\mu\mathrm{W\,cm^{-2}}$ at 0.20 V. Eq. (2) gives an area-normalized maximum-power load of $150\,\Omega\,\mathrm{cm}^2$, while Eq. (3) gives an internal-loss term of approximately $188\,\Omega\,\mathrm{cm}^2$. These values show that the power-producing state is not represented by the open-circuit voltage alone. The cell reaches 0.45 V under open-circuit conditions at high glucose concentration, but usable energy is extracted only when the electrode pair sustains current at a lower voltage.

The voltage utilization ratio $E_{\mathrm{mp}}/E_{\mathrm{OC}}$ is 0.44. This means that less than half of the open-circuit potential is retained at the maximum-power condition. In a printed enzymatic cell, such a drop is expected because the operating current passes through a sequence of coupled processes: glucose diffusion into the enzyme-containing bioanode, mediated electron transfer through naphthoquinone sites, electron percolation through carbon junctions, enzymatic formation of peroxide at the cathodic branch, Prussian-blue-assisted peroxide reduction, and ionic motion through a hydrated polymer/carbon matrix. The load-adaptive calculation is therefore more informative than a simple voltage statement. It identifies a power-oriented load region while also revealing that analytical voltage sensing may need a different load if calibration stability is prioritized over peak power.

Table 2. Calculated load, kinetic, and transport quantities for the flexible glucose biofuel cell.

Quantity	Calculated value	Interpretation
Maximum-power current density, j_{mp}	1.33 mA cm^{-2}	Current-density target at the peak-power point
Maximum-power load-area term, $r_{L,mp}$	150 Ω cm^2	External load region for power-oriented operation
Internal-loss term, r_{int}	188 Ω cm^2	Area-normalized loss associated with reaction and film limitations
Voltage utilization, E_{mp}/E_{OC}	0.44	Fraction of open-circuit voltage retained at maximum power
Kinetic-balance factor, Θ_K	0.995	Strong affinity matching between bioanode and biocathode
Cathode/anode sensitivity ratio	64.9	Cathodic peroxide-linked pathway dominates amperometric gain
Cathode/anode high-rate capacitance-retention ratio	2.91	Cathodic composite retains a larger high-rate charge-storage fraction

Table 2 condenses the central numerical answer of the work. The maximum-power load and internal-loss terms are similar in magnitude, indicating that the external circuit and the printed electrochemical structure jointly determine the usable output. The near-unity kinetic-balance factor shows that the two enzymatic branches are not severely mismatched, while the capacitance-retention ratio reveals a pronounced materials contrast between the anode and cathode. The table therefore links electrical design, enzyme compatibility, and nanocomposite transport in one interpretive frame.

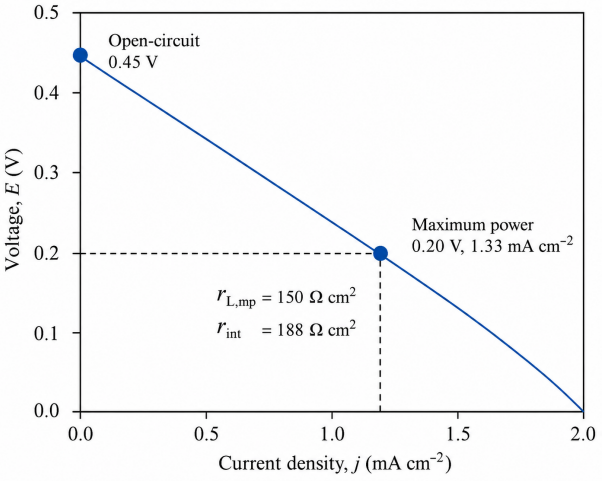

Figure 2. Voltage–current load-line representation of the flexible glucose biofuel cell at high glucose concentration. The plot identifies the open-circuit voltage, the maximum-power operating point, and the resistance-area quantities used to connect electrochemical output with external load selection.

Figure 2 shows the practical consequence of the calculation. The open-circuit point represents charge separation without useful current delivery, whereas the maximum-power point identifies the state where current density and voltage are jointly sufficient for energy extraction. The line also makes clear that selecting an external load much smaller than the matched region would force the cell toward larger current and stronger polarization, while a much larger load would preserve voltage but sacrifice power. For a wearable system, this trade-off matters because the same cell may be used either to harvest energy or to provide a concentration-dependent voltage signal.

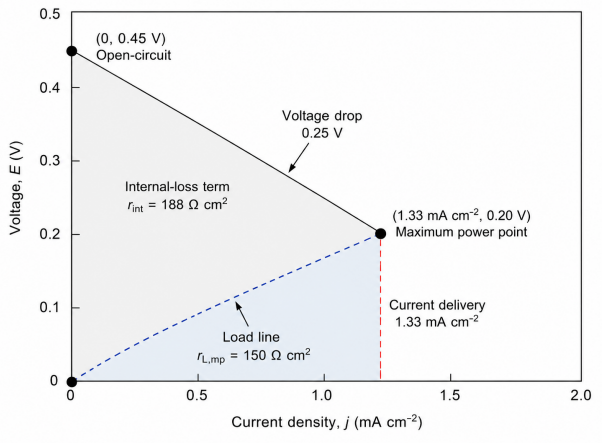

Figure 3. Graphical decomposition of maximum-power operation into load-area and internal-loss contributions. The shaded region and annotated voltage drop show how polarization losses reduce the voltage from open circuit to the current-delivering operating point.

Figure 3 separates the useful load-facing term from the internal loss represented by the drop from 0.45 V to 0.20 V. The approximate 0.25 V difference is not attributable to a single process; it reflects the combined penalty of enzyme kinetics, nanocomposite transport, redox mediation, cathodic peroxide reduction, and contact resistance within a flexible printed network. The value of the figure is therefore diagnostic. It shows that improving output will require both materials refinement and load management, rather than simply increasing the open-circuit voltage.

3.2 Kinetic balance of the single-enzyme electrode pair

The apparent Michaelis constants are 2.47 mM for the bioanode and 2.99 mM for the biocathode. Eq. (4) gives $\Theta_K = 0.995$, which indicates very close affinity compatibility. This value is significant because the two electrodes use the same biological catalyst but different electrochemical roles. The anodic branch converts glucose oxidation into electron flow through the naphthoquinone/carbon network, whereas the cathodic branch relies on glucose oxidase to generate peroxide that is then reduced at Prussian blue. Similar apparent affinity means that the two branches remain active over a comparable concentration interval instead of forcing the cell into a state where one electrode is kinetically saturated while the other still responds strongly.

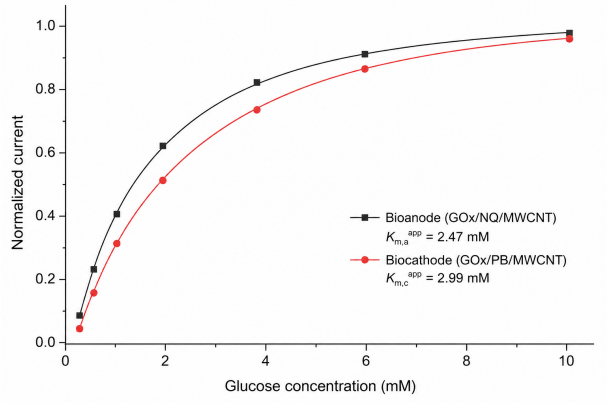

Figure 4. Normalized glucose-response curves of the glucose-oxidase bioanode and biocathode. The apparent Michaelis constants of 2.47 mM and 2.99 mM show that the two enzymatic branches operate within closely aligned glucose-concentration windows despite using different redox materials.

Figure 4 demonstrates that both half-cell responses rise rapidly in the low-millimolar concentration region and approach saturation over similar glucose levels. The anode and cathode curves are not identical, which is expected because the redox mediation mechanisms differ, but their concentration dependence is close enough to support coupled self-powered operation. In practical sensing terms, this means that the cell voltage is less likely to be dominated by a prematurely exhausted half-cell within the investigated sweat-relevant interval.

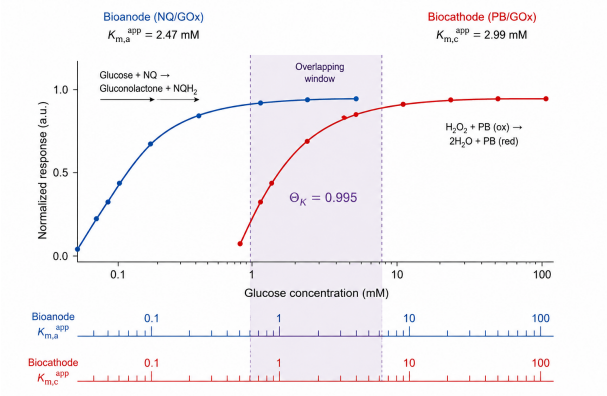

Figure 5. Kinetic-window matching between the bioanode and biocathode. The overlapping response band and the near-unity factor $\Theta_K = 0.995$ indicate that the single-enzyme electrode pair remains kinetically balanced across the relevant glucose range.

Figure 5 places the two apparent Michaelis responses on a shared concentration axis and therefore reveals the overlap that is less obvious when each electrode is considered separately. The shaded region can be interpreted as the concentration zone where both redox branches contribute effectively to cell operation. This overlap is particularly important for a single-

enzyme design because the advantage of reduced biochemical complexity would be lost if the two printed films demanded very different glucose concentrations for efficient function.

The cathodic glucose response is much more sensitive in amperometric mode than the anodic response, with a cathode/anode sensitivity ratio of approximately 64.9. This result should not be interpreted as showing that the anode is unimportant. The anode supplies electrons to the external circuit, while the cathode governs how efficiently the peroxide-linked reduction pathway consumes the oxidizing intermediate and closes the electrochemical loop. The larger cathodic gain indicates that Prussian blue acts as an effective low-potential peroxide transducer. For self-powered sensing, this is advantageous because it strengthens the glucose-dependent cathodic sink without requiring a high external bias that could increase interferent sensitivity.

The kinetic comparison also clarifies the design value of the single-enzyme architecture. Multi-enzyme biofuel cells can be powerful when each electrode is optimized independently, but different enzymes introduce distinct pH preferences, immobilization chemistries, degradation rates, and cost penalties. Here, the near-unity Θ_K value shows that a common glucose-oxidase chemistry can support both fuel oxidation and cathodic signal amplification when paired with appropriately selected redox materials. The result is therefore a materials-integration finding rather than only a biochemical observation.

3.3 Transport behavior of the printed nanocomposites

The scan-rate exponents indicate that neither electrode behaves as a purely diffusion-limited surface nor as a purely surface-confined capacitor. The anodic exponent of 0.58 gives a diffusion-compatibility value of 0.84 using Eq. (5). The cathodic exponents of 0.75 and 0.68 give an average compatibility of approximately 0.57, and the combined cell-level value is approximately 0.71. These values indicate that substrate transport remains a major contributor to the current response, but that surface-associated and capacitive processes become more pronounced in the cathodic Prussian-blue/MWCNT nanocomposite.

This interpretation is reinforced by the high-rate capacitance retention. At $200\,\mathrm{mV\,s^{-1}}$, the cathodic composite retains 63.4% of its areal capacitance, whereas the anodic composite retains 21.8%. The resulting cathode/anode high-rate capacitance-retention ratio is 2.91. In physical terms, the cathodic film preserves a larger fraction of rapid interfacial charge-storage capacity, which may buffer transient load or sweat-contact changes. However, the same feature also warns against transferring calibrations between operating conditions without verification, because the balance between diffusion, catalytic turnover, and capacitive response changes with scan rate, load, and electrolyte state.

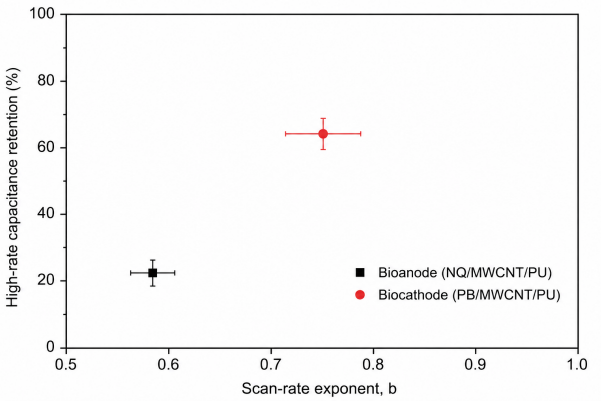

Figure 6. Relationship between scan-rate exponent and high-rate capacitance retention for the bioanode and biocathode nanocomposites. The cathodic Prussian-blue/MWCNT film combines a larger scan-rate exponent with higher capacitance retention, indicating a stronger surface-associated and charge-storage contribution during rapid electrochemical perturbation.

Figure 6 functions as a compact materials map. The anode occupies a region closer to diffusion-compatible current scaling, consistent with mediated glucose oxidation in a printed carbon film. The cathode shifts toward a region with stronger high-rate retention, consistent with the redox-active Prussian-blue/MWCNT interface. This distinction is useful for wearable readout because a rapid change in sweat wetting or external load will not perturb both electrodes in the same way. Calibration and power management should therefore be performed on the complete cell, not inferred from either electrode alone.

3.4 Artificial-sweat voltage calibration

The self-generated voltage in artificial sweat follows a saturating Michaelis-type relation. The fitted expression is

$$E(C) = 49.9 + \frac{30.7\,C}{4.8 + C}, \tag{7}$$

where E is expressed in millivolts and C is glucose concentration in millimoles per litre. Eq. (7) gives a load-dependent offset of 49.9 mV, a maximum incremental voltage term of 30.7 mV, and an apparent half-increment concentration of 4.8 mM. The R^2 value of 0.9737 indicates that the saturating expression captures the dominant trend over 0 mM to 10 mM glucose. The half-increment parameter should be treated as a cell-level calibration constant rather than as a direct enzymatic Michaelis constant, because the measured voltage also depends on polarization, electrode balance, load, and artificial-sweat composition.

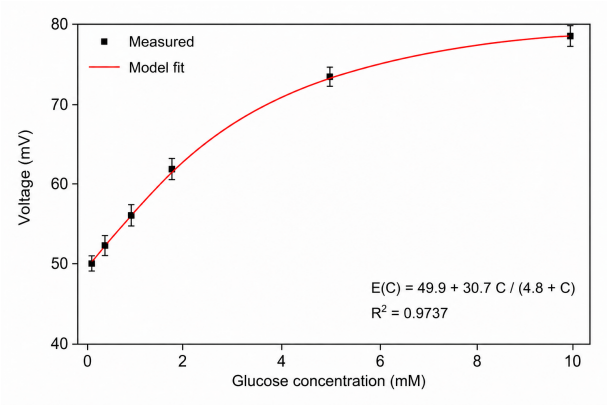

Figure 7. Artificial-sweat voltage calibration of the self-powered glucose biofuel cell. The measured points follow the fitted saturation relation $E(C) = 49.9 + 30.7C/(4.8 + C)$ with $R^2 = 0.9737$, confirming a monotonic voltage-mode response over the investigated glucose range.

Figure 7 answers the analytical part of the research question. The response is monotonic and saturating, which is appropriate for voltage-mode self-powered glucose sensing, but it is not linear over the entire range. The steepest voltage change occurs at lower glucose concentrations, where readout resolution and drift control are most important. At higher concentrations the curve approaches a plateau, so improved analytical discrimination would depend less on increasing the voltage span and more on stabilizing the load, hydration state, and electrode balance. This behavior explains why maximum-power operation and voltage-mode sensing should be treated as related but distinct modes of use.

The calibration result also has a practical implication for wearable electronics. A circuit designed only to maximize harvested power near the 150 $\Omega\,cm^2$ load-area term may not be the best circuit for resolving small voltage changes in the lower glucose interval. Conversely, a high-impedance voltage readout that preserves analytical sensitivity may not extract maximum power. The material system therefore requires mode-aware operation: load matching for energy delivery, stable voltage monitoring for biosensing, and recalibration after severe mechanical deformation or electrolyte-state changes.

3.5 Selectivity, bending endurance, and wearable relevance

A flexible sweat biosensor must preserve glucose readability in the presence of common interferents. The examined interferents were lactate at 14 mM, uric acid at 59 µM, ascorbic acid at 10 µM, and creatinine at 84 µM. The self-powered response changed only slightly after these additions, whereas glucose additions produced distinct signal increments. This result is consistent with glucose-oxidase specificity and with the absence of a large externally applied oxidation potential that could promote nonspecific reactions. It supports the interpretation of the cell as an autonomous biochemical transducer rather than as a conventional biased amperometric electrode.

Figure 8 shows that the major voltage steps are produced by glucose rather than by the selected interferents. The small perturbations after interferent addition are important because they represent the realistic background against which sweat glucose must be read. The subsequent glucose-induced increments demonstrate that the device preserves analyte specificity under the chosen self-powered load condition. This finding strengthens the case for voltage-mode operation, especially where minimizing applied bias helps suppress broad electrochemical oxidation of coexisting sweat components.

Mechanical tolerance is equally important for a wearable material. Under repeated bending, the resistance ratio remained within approximately 0.9–1.1 at 90° and 0.8–1.2 at 180°, returning close to its initial state after relaxation. During electrochemical bending tests at 180°, the device maintained stable output up to about 90 cycles and preserved more than 83% of response after 100 cycles. These values indicate that the polyurethane-supported carbon network can

recover a sufficient fraction of interparticle contact after large deformation. The residual loss after repeated extreme bending is still meaningful, because it implies that long-duration use should include deformation-aware calibration or periodic reference checks.

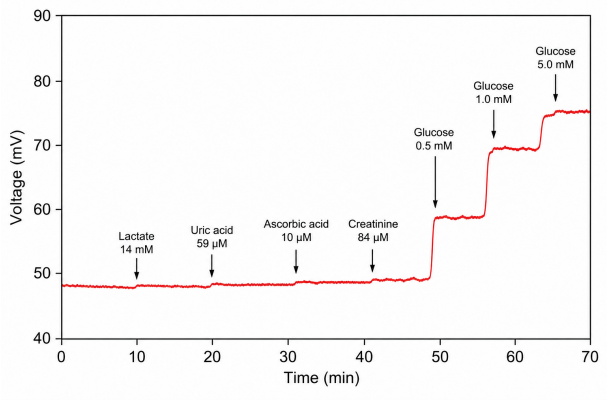

Figure 8. Self-powered voltage response during sequential interferent and glucose additions in artificial sweat. Lactate, uric acid, ascorbic acid, and creatinine cause only minor perturbations, whereas glucose additions produce clear stepwise voltage increments.

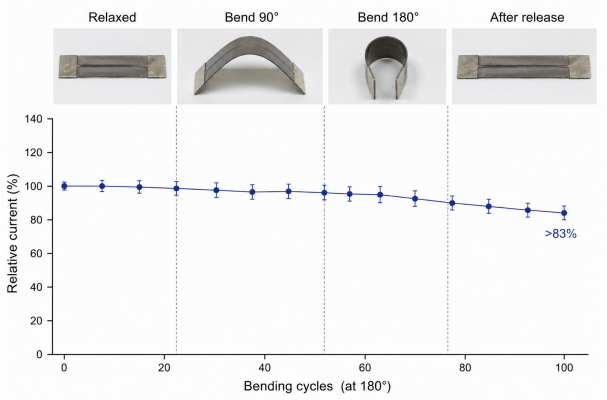

Figure 9. Mechanical bending endurance of the printed flexible biofuel cell. Device images show relaxed, 90°, 180°, and released states, while the current-retention trace demonstrates that more than 83% of the electrochemical response remains after 100 bending cycles at 180°.

Table 3. Operational rules obtained from the normalized load, kinetic, transport, selectivity, and bending quantities.

Operating objective	Governing quantity	Practical rule
Peak energy harvesting	$r_{\mathrm{L,mp}}$ and r_{int}	Select a load near the maximum-power load-area term and minimize additional series/contact resistance.
Voltage-mode biosensing	Saturating relation $E(C)$	Use a stable load and voltage resolution that preserve the steep low-concentration region.
Balanced single-enzyme operation	Θ_K	Maintain immobilization conditions that keep anodic and cathodic apparent Michaelis constants close.
Transport-aware calibration	Ψ_q and capacitance retention	Calibrate under the intended load, scan history, and electrolyte state because diffusion and capacitive contributions differ between electrodes.
Mechanically compliant use	Bending-retention factor	Treat repeated 180° bending as a severe design stress and recalibrate after extensive deformation.
Interferent resistance	Self-powered selectivity response	Avoid unnecessary applied bias so that enzymatic specificity and low-potential cathodic conversion dominate the signal.

Figure 9 links visible deformation to electrochemical retention. The images confirm that the film experiences a severe curvature state, not only a mild flexing condition, while the current-retention trace shows that the output decreases gradually rather than failing abruptly. This behavior suggests that deformation mainly introduces progressive contact

and transport penalties rather than catastrophic film delamination. For wearable use, the implication is clear: the material is mechanically viable for bending-dominated operation, but the calibration should not be assumed permanent after extensive flexural cycling.

Table 3 converts the numerical findings into use rules for device design. The central point is that no single operating condition satisfies all objectives. The maximum-power region is appropriate for energy harvesting, whereas voltage-mode glucose sensing requires a stable calibration and sufficient low-concentration resolution. Kinetic balance must be preserved during enzyme immobilization, transport behavior must be checked under the relevant load and electrolyte state, and bending endurance must be treated as a calibration variable rather than as a simple pass/fail mechanical test.

3.6 Materials-design implications for flexible self-powered sensing

The normalized results show that the flexible single-enzyme glucose biofuel cell can operate as a designable self-powered sweat sensor within the examined concentration, load, and bending ranges. Four findings support this answer. First, the maximum-power point defines a concrete external-load region, with $r_{\mathrm{L,mp}} = 150\,\Omega\,\mathrm{cm}^2$, rather than leaving circuit selection to open-circuit voltage alone. Second, the internal-loss term of $188\,\Omega\,\mathrm{cm}^2$ shows that the printed electrochemical structure imposes a substantial polarization penalty, making materials refinement and load matching equally important. Third, the near-unity Θ_K value demonstrates that a single-enzyme electrode pair can remain kinetically balanced when different redox materials are assigned to the anode and cathode. Fourth, the transport and bending results show that calibration must remain tied to the actual mechanical and electrochemical state of the flexible film.

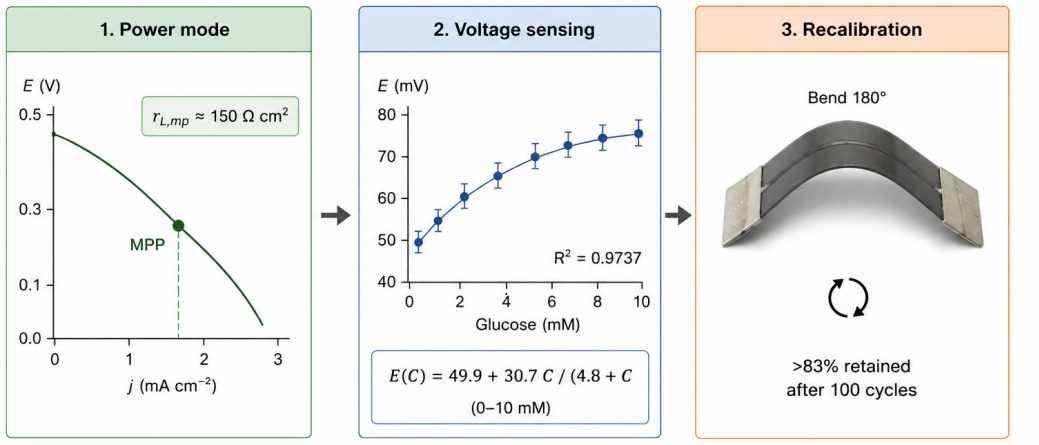

Figure 10. Practical operating sequence for the flexible self-powered glucose biofuel cell. The workflow separates maximum-power operation, voltage-mode glucose sensing, and post-deformation recalibration so that energy harvesting, analytical response, and mechanical recovery are evaluated under their proper conditions.

Figure 10 summarizes the operational logic that follows from the entire analysis. The cell should first be characterized under a power-oriented load when energy delivery is required. It should then be calibrated under the voltage-mode condition intended for sweat glucose sensing. Finally, it should be checked after severe bending because deformation can alter contact resistance, wet-film transport, and voltage stability. The sequence is not merely procedural; it reflects the material physics of the device, where redox chemistry, carbon-network percolation, hydration, and mechanical recovery determine the self-powered signal.

The materials significance of the device lies in the integration of multiwalled carbon nanotubes, naphthoquinone, Prussian blue, polyurethane-supported printed films, and glucose-oxidase interfaces into one mechanically compliant energy-conversion architecture. The analysis shows that this architecture should be judged not only by the magnitude of its power density but also by whether it provides a matched kinetic window, a stable artificial-sweat voltage curve, resistance to selected interferents, and recoverable performance after deformation. In this sense, the printed cell contributes to functional nanostructured electrochemical materials for wearable self-powered biosensing rather than to isolated glucose detection alone.

4 Conclusion

This paper asked whether a flexible printed single-enzyme glucose biofuel cell can be evaluated through a load-adaptive normalization that explains energy harvesting and sweat biosensing within one coherent materials framework. The answer is yes, but with an important condition: the device must be interpreted as a coupled electrochemical, transport, mechanical, and load-dependent system rather than as a sensor described by open-circuit voltage or maximum power alone. At

20 mM glucose, the cell produces 266 µW cm^{-2} at 0.20 V, corresponding to $j_{mp} = 1.33$ mA cm^{-2}, $r_{L,mp} = 150\,\Omega\,cm^2$, and $r_{int} = 188\,\Omega\,cm^2$. These values establish the operating load required for power delivery and quantify the internal polarization penalty imposed by the printed enzymatic material.

The kinetic analysis provides a second part of the answer. Apparent Michaelis constants of 2.47 mM for the bioanode and 2.99 mM for the biocathode give $\Theta_K = 0.995$, demonstrating that the naphthoquinone/MWCNT and Prussian-blue/MWCNT electrodes remain closely matched despite using different redox pathways. This finding supports the feasibility of a single-enzyme glucose-oxidase architecture, provided that the immobilized enzyme environment and redox materials preserve comparable apparent glucose affinity at both electrodes. The transport analysis adds a necessary qualification: the cathodic composite has a stronger surface-associated and capacitance-retaining character than the anodic composite, so calibration cannot be transferred casually between loads, scan histories, or electrolyte states.

The artificial-sweat voltage result completes the biosensing answer. The self-generated voltage follows a saturating expression over 0 mM to 10 mM glucose with $R^2 = 0.9737$, confirming a monotonic, bias-free glucose response. Interferent additions produce only minor voltage perturbations compared with glucose steps, and the printed film retains more than 83% of electrochemical response after 100 repeated 180° bending cycles. The device can therefore function as a flexible self-powered sweat-glucose transducer, but reliable use requires mode-specific operation: load matching for energy extraction, stable voltage calibration for analytical readout, and recalibration or validation after severe deformation. The broader contribution is a normalization route that links nanocomposite electrode design, enzyme compatibility, transport state, and wearable-device operation in a form suitable for evaluating future flexible biofuel-cell sensors.

Data availability

All numerical values required to reproduce the calculations are listed in Tables 1 and 2, together with the fitted voltage expression in Eq. (7).

Conflict of interest

The author declares no conflict of interest.

References

[1] M. Grattieri, S.D. Minteer, Self-powered biosensors. *ACS Sensors, 3*, 44–53 (2018).

[2] I. Jeerapan, J.R. Sempionatto, J. Wang, On-body bioelectronics: wearable biofuel cells for bioenergy harvesting and self-powered biosensing. *Adv. Funct. Mater., 30*, 1906243 (2020).

[3] S. Khumngern, I. Jeerapan, Synergistic convergence of materials and enzymes for biosensing and self-sustaining energy devices towards on-body health monitoring. *Commun. Mater., 5*, 135 (2024).

[4] J. Moyer, D. Wilson, I. Finkelshtein, B. Wong, R. Potts, Correlation between sweat glucose and blood glucose in subjects with diabetes. *Diabetes Technol. Ther., 14*, 398–402 (2012).

[5] C.J. Harvey, R.F. LeBouf, A.B. Stefaniak, Formulation and stability of a novel artificial human sweat under conditions of storage and use. *Toxicol. In Vitro, 24*, 1790–1796 (2010).

[6] Z. Fredj, G. Rong, M. Sawan, Recent advances in enzymatic biofuel cells to power up wearable and implantable biosensors. *Biosensors, 15*, 218 (2025).

[7] N. Mano, Engineering glucose oxidase for bioelectrochemical applications. *Bioelectrochemistry, 128*, 218–240 (2019).

[8] P. Pinyou, V. Blay, L.M. Muresan, T. Noguer, Enzyme-modified electrodes for biosensors and biofuel cells. *Mater. Horiz., 6*, 1336–1358 (2019).

[9] B. Reuillard, A. Le Goff, C. Agnès, M. Holzinger, A. Zebda, C. Gondran, K. Elouarzaki, S. Cosnier, High power enzymatic biofuel cell based on naphthoquinone-mediated oxidation of glucose by glucose oxidase in a carbon nanotube 3D matrix. *Phys. Chem. Chem. Phys., 15*, 4892–4896 (2013).

[10] A.A. Karyakin, Prussian blue and its analogues: electrochemistry and analytical applications. *Electroanalysis, 13*, 813–819 (2001).

[11] K. Veenuttranon, K. Kaewpradub, I. Jeerapan, Screen-printable functional nanomaterials for flexible and wearable single-enzyme-based energy-harvesting and self-powered biosensing devices. *Nano-Micro Lett., 15*, 85 (2023).

[12] J. Cai, F. Shen, J. Zhao, X. Xiao, Enzymatic biofuel cell: A potential power source for self-sustained smart textiles. *iScience, 27*, 108998 (2024).

[13] N. Gao, G. Xu, G. Chang, Y. Wu, From lab to life: self-powered sweat sensors and their future in personal health monitoring. *Adv. Sci., 12*, e2409178 (2025).

[14] H. Wu, Y. Zhang, A.L. Kjøniksen, X. Zhou, X. Zhou, Wearable biofuel cells: advances from fabrication to application. *Adv. Funct. Mater., 31*, 2103976 (2021).

[15] K. Chansaenpak, A. Kamkaew, S. Lisnund, P. Prachai, P. Ratwirunkit, T. Jingpho, V. Blay, P. Pinyou, Development of a sensitive self-powered glucose biosensor based on an enzymatic biofuel cell. *Biosensors, 11*, 16 (2021).

[16] S. Hao, Y. Sun, B. Zhang, X. Zhang, A mediator-free self-powered glucose biosensor based on a hybrid glucose/MnO_2 enzymatic biofuel cell. *Nano Research, 14*, 1827–1835 (2021).

[17] K. Itaya, T. Ataka, S. Toshima, Spectroelectrochemistry and electrochemical preparation method of Prussian blue modified electrodes. *J. Am. Chem. Soc., 104*, 4767–4772 (1982).

[18] A.F. Yeknami, X. Wang, I. Jeerapan, S. Imani, A. Nikoofard, J. Wang, P.P. Mercier, A 0.3-V CMOS biofuel-cell-powered wireless glucose/lactate biosensing system. *IEEE J. Solid-State Circuits, 53*, 3126–3139 (2018).

[19] A.J. Bandodkar, P. Gutruf, J. Choi, K. Lee, Y. Sekine et al., Battery-free, skin-interfaced microfluidic/electronic systems for simultaneous electrochemical, colorimetric, and volumetric analysis of sweat. *Sci. Adv., 5*, eaav3294 (2019).

[20] N. Elgrishi, K.J. Rountree, B.D. McCarthy, E.S. Rountree, T.T. Eisenhart, J.L. Dempsey, A practical beginner's guide to cyclic voltammetry. *J. Chem. Educ., 95*, 197–206 (2018).

[21] S. Zhang, M. Wang, L. Jiang, H. Zhang, The application of wearable glucose sensors in point-of-care testing. *Front. Bioeng. Biotechnol., 9*, 774210 (2021).